

# Reconsidering the Energy Efficiency of Spiking Neural Networks Inference from Analytical Perspectives

Zhanglu Yan, Zhenyu Bai\*, Kaiwen Tang and Weng-Fai Wong, *Senior Member, IEEE*

**Abstract**—Spiking Neural Networks (SNNs) promise higher energy efficiency over conventional Quantized Artificial Neural Networks (QNNs) due to their event-driven, spike-based computation. However, prevailing energy evaluations often oversimplify, focusing on computational aspects while neglecting critical overheads like comprehensive data movement and memory access. Such simplifications can lead to misleading conclusions regarding the true energy benefits of SNNs. This paper presents a rigorous re-evaluation. We establish a fair baseline by mapping rate-encoded SNNs with  $T$  timesteps to functionally equivalent QNNs with  $\lceil \log_2(T + 1) \rceil$  bits. This ensures both models have comparable representational capacities, as well as similar hardware requirement, enabling meaningful energy comparisons. We introduce a detailed analytical energy model encompassing core computation and data movement. Using this model, we systematically explore a wide parameter space, including intrinsic network characteristics ( $T$ , spike rate  $s_r$ , QNN sparsity  $\gamma$ , model size  $N$ , weight bit-level) and hardware characteristics (memory system and network-on-chip). Our analysis identifies specific operational regimes where SNNs genuinely offer superior energy efficiency. For example, under typical neuromorphic hardware conditions, SNNs with moderate time windows ( $T \in [5, 10]$ ) require an average spike rate ( $s_r$ ) below 6.4% to outperform equivalent QNNs. Furthermore, to illustrate the real-world implications of our findings, we analyze the operational lifetime of a typical smartwatch, showing that an optimized SNN can nearly double its battery life compared to a QNN. These insights guide the design of truly energy-efficient neural network solutions.

**Index Terms**—Spiking neural network, Quantized neural network, Energy efficiency

## I. INTRODUCTION

Spiking Neural Networks, characterized by event-driven sparsity and binary spike signaling, represent a compelling approach in neuromorphic computing. Unlike conventional ANNs that process dense tensors, SNNs transmit sparse binary spike trains using *integrate-and-fire* (IF) model, significantly reducing computational load and promising substantial energy savings [1]–[4]. As shown in Figure 1, at each timestep  $t$ , the SNN neuron calculates the weighted sum of incoming spikes, adds this to a accumulated membrane potential,  $V$ , from the previous timestep  $t - 1$ , and checks it against a threshold  $\theta$ . If the threshold is exceeded, the neuron emits a spike ‘1’ and resets the potential. Otherwise, it outputs a ‘0’ [5], [6]. Recent architectures such as SpikingFormer [7], SpikingBERT [8], SpikeLM [9], and Sorbet [10] demonstrate

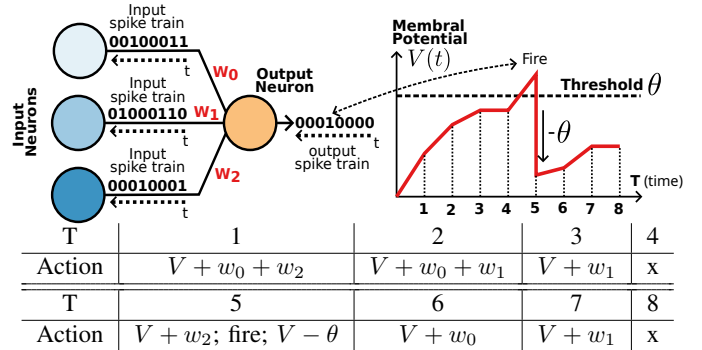


Fig. 1: Integrate-and-fire SNN model

successful integration of spiking dynamics in complex models, including large language models, showcasing notable energy reductions.

However, accurately realizing these energy benefits is complex [11]. Prevailing evaluations often rely on simplistic metrics, such as counting number of additions versus multiplications and assuming a fixed energy consumption per addition and multiplication [12]. The cost of the data movements is one of the critical factors but often overlooked: due to the poor scalability of memories (commonly known as the memory wall [13]), the energy consumption of memory operations becomes even dominating over the energy spent by the computations themselves [14], [15]. While SNNs often claim to be event-driven [16], therefore leverages spike-train sparsity to skip computations, this mechanism require multiple data accesses per neuron activation cycles ( $T \times s_r$  times per weight, where  $T$  is the time window size and  $s_r$  is the spike rate), unlike ANNs that typically fetch weights just once per activation. This increased memory access, along with data movements for spikes, can significantly impact the energy consumption, calling the energy efficiency of SNNs into question. Thus, this paper addresses this critical question: **Under what specific algorithmic and hardware conditions do SNNs achieve genuinely superior end-to-end energy efficiency compared to ANNs?**

Evaluating the end-to-end energy efficiency of neural network inference is a multifaceted challenge, influenced by interacting factors spanning model design (software), software-to-hardware mapping (or compilation), and the specifics of the underlying hardware architecture and their physical implementation. Ensuring a fair, “apples-to-apples” comparison

Zhanglu Yan, Zhenyu Bai, Kaiwen Tang and Weng-Fai Wong are with the School of Computing, National University of Singapore. {zhangluyan, wongwf}@comp.nus.edu.sg

\*Corresponding author.

between different neural network paradigms, such as SNNs and conventional ANNs, is therefore inherently complex. To enable a fair comparison, our approach exploits a key observation: each rate-encoding SNN has a near-equivalent Quantized ANN counterpart that we call the **QNN-SNN twin**. These twins share the same network structure and weight datatype, differing only in their activation representations. Leveraging this equivalence enables controlled comparison across varied model architecture settings and hardware settings.

### A. The QNN-SNN Twins

Our comparison is based on the fundamental observation that a rate-encoding SNN can always be converted to a near-equivalent QNN, and vice versa. Specifically, an SNN operating over  $T$  timesteps is paired with a QNN with the same network structure but utilizing activations quantized to  $\lceil \log_2(T + 1) \rceil$  bits. These QNN-SNN twins share the same network structure and weight datatype, differing only in their activation representation and computation methods. Because of such identity, we can keep consistent hardware mapping for the twin. Consequently, when comparing twin QNN-SNN pairs, we control both the model capability and mapping, isolating hardware differences and how the twin can be executed on that hardware as the primary factors.

### B. Hardware Energy Consumption

Hardware inference energy consumption comprises three primary components:

$$E = E_{\text{Compute}} + E_{\text{Data}} (+E_{\text{Control}}) \quad (1)$$

**Compute Energy ( $E_{\text{Compute}}$ ):** This accounts for energy spent on arithmetic operations—additions in SNNs and multiplications plus additions in ANNs—and activation functions. Although SNNs replace multiplications with additions, potentially saving energy due to sparsity, actual energy savings depend on specific hardware implementations, arithmetic designs, operand data types, and the operational sparsity level.

**Data Movement Energy ( $E_{\text{Data}}$ ):** Digital hardware fundamentally relies on moving data between and among storage (memories) and compute units, performing computations, and subsequently transferring data to the next computation stage or output. Specifically, for SNN and QNN architectures, this includes fetching weights and transferring intermediate activations.

On digital devices, data movement typically occurs through memory hierarchies or Network-on-Chip (NoC). The resulting data traffic depends heavily on both hardware characteristics and the model-to-hardware mapping. Our analysis primarily targets spatial dataflow architectures where data movement predominantly occurs via NoCs rather than memory hierarchies. Neuromorphic architectures can be considered a subset of these dataflow architectures. While neuromorphic architectures are specialized for SNN workloads, general dataflow platforms (e.g., Tenstorrent [17], Cerebras [18], SambaNova [19]) support broader AI tasks. Therefore, our analytical model is generalized beyond specific neuromorphic hardware.

**Control Energy ( $E_{\text{Control}}$ ):** General-purpose architectures typically invest hardware resources either at the front-end to support unified programming interfaces—such as instruction fetching and decoding for Instruction Set Architectures (ISAs)—or at the back-end to enhance performance across diverse applications, such as out-of-order buffers in CPUs and warp schedulers in GPUs. In this study, we exclude these architectural costs related to generality-specialization trade-offs because we mostly focus on specialized architecture where this control cost is low. In other words, we are trying to find out what kind of specialization is more (or less) beneficial for SNN. Instead, our analysis focuses on compute and data movement costs.

### C. Key contributions

The key contributions are summarized as follows:

- We develop a comprehensive analytical energy model to compare SNNs against equivalent QNNs, which systematically accounts for core computation and data movements (including weights, sparse and dense activations).
- We conduct two energy analyses. First, we map the  $E_{\text{SNN}}/E_{\text{QNN}}$  energy ratio across a broad landscape of SNN model configurations and hardware cost scenarios to provide a high-level overview of when SNN is better. Second, we perform a focused sensitivity analysis under typical neuromorphic settings to identify and quantify the impact of critical network parameters ( $T$ ,  $s_r$ , weight precision, and  $N_{\text{src}}$ ) on relative energy efficiency.
- Based on our findings, we delineate the specific conditions under which SNNs achieve an energy advantage over QNNs, providing clear guidance for model selection and hardware-software co-design in energy-constrained systems.

The remainder of this paper is organized as follows. Section II first establishes the principle of information representation equivalence between SNNs and QNNs, which provides a fair basis for our comparison. Section III then develops our analytical energy models, detailing the formulas for computation and data movement for both network types. In Section IV, we leverage these models to conduct a comprehensive energy analysis across various network configurations and hardware settings. Finally, Section V discusses the future research directions and the potential for SNNs on energy-constrained devices. In conclusion, this paper presents a comprehensive analysis that re-evaluates the energy efficiency of SNNs. By detailing the specific network structure and hardware conditions under which SNNs hold a true energy advantage, our work provides a guiding framework for the design of energy-efficient SNNs.

## II. INFORMATION REPRESENTATION EQUIVALENCE BETWEEN SNN AND ANN

To establish a fair basis for comparing SNNs and QNNs, we first demonstrate their equivalence in terms of information representation capability. Theorem 1 establishes that a rate-encoded IF-based SNN has a QNN counterpart with a specific activation precision. Subsequently, Theorem 2 formalizes the

relationship between the SNN's spike rate and the QNN's activation sparsity.

**Theorem 1.** *For a rate-encoded IF SNN operating with a time window of size  $T$ , there exists an equivalent QNN whose activations are quantized to at most  $\lceil \log_2(T+1) \rceil$  bits, such that both networks possess a comparable information representation capability at the single neuron output level.*

*Proof Outline.* The argument proceeds as follows: Lemma 1 first establishes that the membrane potential  $v(t)$  of an IF neuron remains bounded within  $[0, \theta)$  under typical input condition. This ensures that the residual potential  $v(T)$  at the end of the time window  $T$  is also within this range. Building upon this, Lemma 2 demonstrates that the influence of this bounded residual potential  $v(T)$  on the total output spike count is assumed to be negligible, then the SNN's  $T+1$  discrete output levels (normalized spike counts) can be matched by a QNN employing at most  $\lceil \log_2(T+1) \rceil$  bits. Finally, Corollary 1 addresses scenarios where the simplifying assumption regarding  $v(T)$ 's negligible impact does not fully hold. In such non-ideal cases, the SNN's effective information representation capacity does not exceed, and may indeed be less than, that of the  $\lceil \log_2(T+1) \rceil$ -bit QNN. Collectively, these steps justify Theorem 1 by showing that the QNN with  $\lceil \log_2(T+1) \rceil$  bits serves as a robust upper bound or equivalent benchmark for the SNN's representational capability.  $\square$

**Lemma 1.** *Consider an IF neuron without leakage and employing a reset-by-subtraction mechanism with a firing threshold  $\theta$ . If at each timestep  $t \in [1, T]$ , the net input current  $I(t)$  (i.e.,  $\sum_j w_j s_j(t)$ ) satisfies  $0 \leq I(t) < \theta$ , then the membrane potential  $v(t)$  remains bounded such that  $0 \leq v(t) < \theta$  for all  $t \in [1, T]$ , assuming  $v(0) = 0$ .*

*Proof.* The membrane potential  $v(t)$  evolves as  $v(t) = v(t-1) + I(t) - \theta s_{\text{out}}(t)$ , where  $s_{\text{out}}(t) \in \{0, 1\}$  is the output spike at timestep  $t$ , and  $v(0) = 0$ . We prove  $0 \leq v(t) < \theta$  by induction on  $t$ . **Base case** ( $t = 0$ ):  $v(0) = 0$ , so  $0 \leq v(0) < \theta$  holds. **Inductive step:** Assume  $0 \leq v(t-1) < \theta$  for some  $t \geq 1$ . At timestep  $t$ :

- **No spike emitted** ( $s_{\text{out}}(t) = 0$ ): This occurs if  $v(t-1) + I(t) < \theta$ . Then,  $v(t) = v(t-1) + I(t)$ . Since  $v(t-1) \geq 0$  and  $I(t) \geq 0$ ,  $v(t) \geq 0$ . By the condition for no spike,  $v(t) < \theta$ . Thus,  $0 \leq v(t) < \theta$ .
- **Spike emitted** ( $s_{\text{out}}(t) = 1$ ): This occurs if  $v(t-1) + I(t) \geq \theta$ . Then,  $v(t) = v(t-1) + I(t) - \theta$ . Since  $v(t-1) + I(t) \geq \theta$ , it follows that  $v(t) \geq 0$ . Furthermore, given  $v(t-1) < \theta$  (by induction hypothesis) and  $I(t) < \theta$  (by premise), we have  $v(t-1) + I(t) < 2\theta$ . Therefore,  $v(t) = v(t-1) + I(t) - \theta < 2\theta - \theta = \theta$ . Thus,  $0 \leq v(t) < \theta$ .

In both cases,  $0 \leq v(t) < \theta$  holds, completing the induction.  $\square$

**Lemma 2.** *Assume an IF neuron model receiving input spike trains  $s_j(t)$  with weights  $w_j$  over  $T$  timesteps. Let  $k_j = \sum_{t=1}^T s_j(t)$  be the total input spikes on channel  $j$ . If the conditions of Lemma 1 are met (ensuring  $0 \leq v(T) < \theta$ ), then the SNN's output representation ability can be matched*

*by a QNN whose activation function produces  $\lceil \log_2(T+1) \rceil$  distinct levels.*

*Proof.* The dynamics of the membrane potential are  $v(t) = v(t-1) + \sum_j w_j s_j(t) - \theta s_{\text{out}}(t)$ , with  $v(0) = 0$ . Summing this relation from  $t = 1$  to  $T$  yields:

$$\sum_{t=1}^T (v(t) - v(t-1)) = \sum_{t=1}^T \sum_j w_j s_j(t) - \sum_{t=1}^T \theta s_{\text{out}}(t).$$

The left side is a telescoping sum,  $v(T) - v(0)$ . Let  $n = \sum_{t=1}^T s_{\text{out}}(t)$  be the integer count of output spikes, and  $k_j = \sum_{t=1}^T s_j(t)$  be the total input spikes from presynaptic neuron  $j$ . Since  $v(0) = 0$ , we have:

$$v(T) = \sum_j w_j k_j - \theta n.$$

Rearranging for  $n$ , which is an integer by definition:

$$\theta n = \sum_j w_j k_j - v(T) \implies n = \frac{\sum_j w_j k_j - v(T)}{\theta}.$$

Let  $X = \frac{\sum_j w_j k_j}{\theta}$  and  $\epsilon = \frac{v(T)}{\theta}$ . The equation becomes  $n = X - \epsilon$ , which implies  $X = n + \epsilon$ . Under the conditions of Lemma 1,  $0 \leq v(T) < \theta$ , which implies  $0 \leq \epsilon < 1$ . Since  $n$  is an integer and  $0 \leq \epsilon < 1$ ,  $\lfloor x \rfloor = m \iff m \leq x < m+1$  for integer  $m$ , directly yields  $n = \lfloor X \rfloor$ . Therefore, the number of output spikes is given exactly by:

$$n = \left\lfloor \frac{\sum_j w_j k_j}{\theta} \right\rfloor.$$

The SNN's average output firing rate is  $\phi_{\text{SNN}}(T) = n/T$ . An SNN neuron can produce integer spike counts  $n \in \{0, 1, \dots, T\}$ . This results in  $T+1$  distinct output levels. For an equivalent QNN, let its input activations be  $a_j = k_j/T$ . The QNN computes a pre-activation  $z_{\text{QNN}} = \sum_j w_j a_j = (\sum_j w_j k_j)/T$ . We can build a QNN's activation function  $h(z_{\text{QNN}})$  to map the output of SNN exactly:

$$h(z_{\text{QNN}}) = \frac{1}{T} \left\lfloor \frac{z_{\text{QNN}} \cdot T}{\theta} \right\rfloor = \frac{1}{T} \left\lfloor \frac{\sum_j w_j k_j}{\theta} \right\rfloor = \frac{n}{T}.$$

To represent these  $T+1$  distinct values, a QNN requires  $\lceil \log_2(T+1) \rceil$  bits of precision for its output activations.  $\square$

**Corollary 1.** *If the conditions stipulated in Lemma 1 are violated (e.g., if net input current  $I(t) \geq \theta$  for some  $t$ , potentially leading to  $v(T)$  not being constrained within  $[0, \theta)$  in the manner assumed for the exact derivation, or if other factors like synaptic noise or neuronal leakage are significant), the precise relationship  $n = \lfloor (\sum_j w_j k_j)/\theta \rfloor$  may be perturbed. Such deviations can effectively reduce the SNN's encoding precision or introduce stochasticity, ensuring that its*

<sup>1</sup>The function  $h(z)$  is the conversion function from real numbers to fixed-point representation during the quantization aware training process. During inference, the weights are quantized to integers and the activation  $z$  are fix-point values  $\in \frac{\mathbb{N}}{N}$ , where  $N$  is unsigned integers. So,  $h(z)$  function is executed as  $z/\theta$  and  $\theta$  is usually chosen as 1 or a power of 2 [12], [20]. Then this division can be implemented as a bit shift with negligible energy overhead.

useful information representation capacity generally does not exceed that of an idealized QNN with  $\lceil \log_2(T + 1) \rceil$  bits.

**Theorem 2.** Consider a QNN with  $N_{src}$  inputs. Let  $\gamma$  denote its sparsity rate. Since we establish an equivalence with a rate-coded SNN operating over a time window  $T$ , we assume that each non-zero QNN input activation  $a_j$  lies in the range  $[1/T, 1]$ . Here,  $a_j = 1/T$  signifies the minimal non-zero signal (equivalent to one spike event in the SNN over  $T$  timesteps), and  $a_j = 1$  represents the maximal signal (equivalent to SNN events at every discrete opportunity within  $T$ ). If an SNN is to represent the same input information as this QNN using rate coding, its average input spike rate  $s_r$  (defined as the average number of spikes per input neuron per SNN timestep) is bounded by:

$$\frac{1 - \gamma}{T} \leq s_r \leq 1 - \gamma.$$

*Proof.* Let the QNN have  $N_{src}$  input channels. The number of channels with non-zero activations is  $(1 - \gamma)N_{src}$ . Each such non-zero QNN activation  $a_j$  is interpreted as an average rate or signal strength. To represent this input value  $a_j$  using rate coding in an SNN over a time window of  $T$  discrete timesteps, the corresponding input channel  $j$  of the SNN would receive  $k_j = a_j T$  spikes during this window. For input channels where the QNN activation  $a_j = 0$ , the SNN receives  $k_j = 0$  spikes.

The total number of input spikes received by the SNN across all  $N_{src}$  input channels during the window  $T$  is the sum of spikes from active channels:

$$\sum_{j=1}^{N_{src}} k_j = \sum_{j \text{ s.t. } a_j \neq 0} (a_j T) = T \sum_{j \text{ s.t. } a_j \neq 0} a_j.$$

The average SNN input spike rate  $s_r$  is defined as the total input spikes normalized by the total number of input channels and the number of timesteps:

$$s_r = \frac{\sum_{j=1}^{N_{src}} k_j}{N_{src} \cdot T} = \frac{T \sum_{j \text{ s.t. } a_j \neq 0} a_j}{N_{src} \cdot T} = \frac{\sum_{j \text{ s.t. } a_j \neq 0} a_j}{N_{src}}.$$

Let  $N_{active} = (1 - \gamma)N_{src}$  be the number of input channels with non-zero QNN activations. The sum  $\sum_{j \text{ s.t. } a_j \neq 0} a_j$  is bounded. Given the assumption that each of the  $N_{active}$  non-zero activations  $a_j$  is in the range  $[1/T, 1]$ :

- The minimum sum occurs when all  $N_{active}$  activations take the value  $1/T$ :

$$\min \left( \sum_{j \text{ s.t. } a_j \neq 0} a_j \right) = N_{active} \cdot \frac{1}{T} = (1 - \gamma)N_{src} \cdot \frac{1}{T}.$$

- The maximum sum occurs when all  $N_{active}$  activations take the value 1:

$$\max \left( \sum_{j \text{ s.t. } a_j \neq 0} a_j \right) = N_{active} \cdot 1 = (1 - \gamma)N_{src} \cdot 1.$$

Substituting these bounds into the expression for  $s_r$ :

- Minimum  $s_r = \frac{(1 - \gamma)N_{src}(1/T)}{N_{src}} = \frac{1 - \gamma}{T}$ .
- Maximum  $s_r = \frac{(1 - \gamma)N_{src}(1)}{N_{src}} = 1 - \gamma$ .

Thus, we establish the bounds  $\frac{1 - \gamma}{T} \leq s_r \leq 1 - \gamma$ .  $\square$

Based on proof, we analyze three scenarios of spike rates in the following sections given a fixed QNN activation sparsity of  $\gamma$ :

- **Worst-Case for SNN Efficiency (Highest Spike Rate):** This scenario occurs when all  $(1 - \gamma)N_{src}$  active QNN neurons have the maximum activation value,  $a_j = 1$  (equivalent to  $T/T$ ). This corresponds to the SNN receiving  $T$  spikes for every active input. As derived from Theorem 2, this yields the highest possible average spike rate for the SNN:  $s_r^{worst} = 1 - \gamma$ .
- **Best-Case for SNN Efficiency (Lowest Spike Rate):** This occurs when all active QNN neurons have the minimum non-zero activation value,  $a_j = 1/T$ , which corresponds to a single spike event in the SNN for each active input. This results in the lowest possible average spike rate:  $s_r^{best} = (1 - \gamma)/T$ .
- **Average-Case:** We assume the QNN's non-zero activation values are uniformly distributed within the range  $[1/T, 1]$ . The average activation value across active neurons is therefore  $(1/T + 1)/2$ . This leads to an average SNN spike rate of  $s_r^{avg} = \frac{(1 - \gamma)(1/T + 1)}{2}$ .

Conversely, for a given SNN with time window  $T$  and spike rate  $s$ , there exist three corresponding QNNs whose activation sparsity  $\gamma$  of  $1 - s$ ,  $1 - \frac{2sT}{T+1}$ , and  $1 - sT$  represent the worst, average, and best-case scenarios, respectively, for the SNN's relative energy efficiency.

### III. HARDWARE

Section II established our comparative methodology, centered on the principle that for any SNN, a twin QNN with near-equivalent representational capabilities can be defined. This equivalence maintains consistency in weight datatypes and overall network architecture, isolating differences to the representation of activations and the computations required to generate them. Building on this foundation, this section delves into the hardware implications arising from these distinctions. Our primary objective is to deduce the energy trade-offs between SNNs and QNNs, thereby identifying the specific operational conditions and parameter regimes under which one paradigm achieves superior energy efficiency over the other. In the following sections, we consider the energy consumption of a single output neuron with  $N_{src}$  input neurons for both the SNN and the QNN forming a twin SNN-QNN pair. Specifically, the SNN with  $T$  timestep is paired to a QNN with  $\lceil \log_2(T + 1) \rceil$  bits-integer quantization. The latter processes its input in one forward pass with integer multiplication and accumulation while the former spreads computations over  $T$  time steps with additions only. Although SNN are known to be sparse (or the *spike rate* as the density), QNN may also have sparsity due to the sparsification effect of the activation function such as *ReLU*. Let  $\gamma$  be the fraction of zero activations in the QNN (sparsity), and  $s_r$  the average spike rate (density) per input in the SNN (i.e., each input spikes in a fraction  $s$  of the  $T$  steps, matching the ANN's sparsity as per Theorem 2). Our analytical framework is indeed network-agnostic. The structural differences between CNNs and Transformers are captured by our model's core parameters,

primarily  $N_{src}$  (e.g., input channel numbers  $\times$  kernel width and length, for a CNN vs. the FFN dimension for a Transformer).

### A. Core computing ( $E_{Compute}$ )

Core computing energy quantifies the energy consumed by fundamental arithmetic operations. For Artificial Neural Networks, this primarily involves multiply-accumulate (MAC) operations, whereas Spiking Neural Networks predominantly utilize accumulate (ACC) operations.

In a typical ANN layer, core computation consists of summing  $N_{src}$  weighted inputs, followed by a non-linear activation function. This activation often includes clamping to constrain output values to a defined range (e.g.,  $[0,1]$ ). The computational energy for ANNs,  $E_{ANN}^c$ , can thus be expressed as:

$$E_{ANN}^c = N_{src} \cdot \underbrace{(1 - \gamma) \cdot E_{MAC}}_{\text{Active Operations}} + \underbrace{2E_{CMP}}_{\text{Clamping}} \quad (2)$$

where  $E_{MAC}$  is the energy per MAC operation, and  $E_{CMP}$  is the energy per comparison for clamping. Due to the sparsity, only  $(1 - \gamma)$  computations are necessary after skipping the zero activations.

For SNNs employing Integrate-and-Fire neuron models, MACs are replaced by additions (accumulations). The core computational energy for SNNs,  $E_{SNN}^c$ , is given by:

$$E_{SNN}^c = \underbrace{N_{src} \cdot T \cdot s_r \cdot E_{ACC}}_{\text{Membrane Potential Update}} + \underbrace{T \cdot (E_{CMP} + s_r \cdot E_{SUB})}_{\text{Spiking Operations over T}} \quad (3)$$

Here,  $T$  is the number of timesteps,  $s_r$  is the average spike rate,  $E_{ACC}$  is the energy for an accumulation, and  $E_{SUB}$  is the energy for a subtraction (e.g., for membrane potential update after firing).

To compare the computational energy efficiency, we introduce a parameter  $k$ , representing the energy ratio of a MAC operation over an addition. Assuming  $E_{ACC} = E_{CMP} = E_{SUB}$ , we define  $k = E_{MAC}/E_{ACC}$ . An SNN offers computational energy savings if  $E_{SNN}^c \leq E_{ANN}^c$ , which leads to the condition:

$$Ts_r + \frac{T + Ts_r - 2}{N_{src}} \leq k(1 - \gamma) \quad (4)$$

For typical large-scale neural networks,  $N_{src}$  is large (e.g.,  $\geq 10^3$ ), rendering the term  $\frac{T + Ts_r - 2}{N_{src}}$  negligible. This simplifies the condition for SNN computational energy advantage to  $Ts_r \leq k(1 - \gamma)$ .<sup>2</sup> We analyze this simplified condition under three SNN spike rate scenarios discussed in Theorem 2:

- **Best-case for SNN** ( $s_r = \frac{1-\gamma}{T}$ ): Corresponds to the minimum SNN spike rate to match QNN activation density  $(1-\gamma)$  over  $T$  timesteps. SNNs are more computationally energy-efficient if  $k \geq 1$ .
- **Average-case for SNN** ( $s_r = \frac{(1-\gamma)(1/T+1)}{2}$ ): SNNs are favored if  $k \geq \frac{1+T}{2}$ .
- **Worst-case for SNN** ( $s_r = 1 - \gamma$ ): Represents the maximum SNN spike rate, where each potential input effectively triggers a spike in every relevant timestep.

<sup>2</sup>This simplification was used only in Section III.A to provide a high-level intuition; in the later results section, all concrete energy calculations for both ANNs and SNNs were computed using the full, unsimplified energy models presented in Eq. (2) and Eq. (3).

SNNs are favored if  $k \geq T$ . (The referenced study notes  $k > T$  for strict superiority).

### B. Data Movement Energy ( $E_{data}$ )

Data movement between storage, compute units, and among compute units is a fundamental and often dominant component of energy consumption in neural network computations. While classical Von Neumann architectures rely heavily on memory hierarchies (on-chip SRAM, off-chip DRAM) for data transfer, the well-known *memory wall* in silicon-based digital devices has spurred the development of non-Von Neumann approaches. Dataflow architectures, which prioritize efficient data movement through fixed datapaths or NoCs, are prominent examples. However, memory remains indispensable as *storage devices* for storing static information like model weights. Consequently, the data movement energy in NN models primarily comprises the costs of fetching weights and transferring activations. These costs are highly sensitive to hardware technologies (e.g., memory type, NoC design) and mapping strategies, which dictate data transfer distances and patterns.

Many digital neuromorphic architectures (e.g., Loihi [21], TrueNorth [22]) can be categorized as specialized dataflow systems. While often specialized for SNNs, neuromorphic architectures share fundamental similarities with other dataflow systems like Tenstorrent [17], Sambanova [19] and Cerebras [18] that are general architectures for a wide range of tasks including AI and other HPC workloads.

Since dataflow architectures generally require static mapping, we consider a common mapping strategy for SNN where weights are stored locally within each *core's* SRAM, and activations are shared across cores via a dedicated NoC, as illustrated in the archetypal architecture shown in Figure 2. Each core integrates local memory, control logic, and compute units for ordered task execution. This is also the reason we prioritize dataflow architecture over other spatial architectures such as GPUs because the latter have complex dynamic schedule and memory behavior that are hard to be controlled for a fair and accurate comparison between the SNN-QNN twins. Although this *weight-stationary* mapping is not necessarily the optimal mapping for SNN or QNN depending on the datatype and the model architecture, this mapping can ensure a fair comparison between SNN and the twin QNN.

We need to further distinguish the energy consumption of moving activations by moving sparse activation and dense activation. We denote  $\bar{E}^{\text{move}}$  and  $\tilde{E}^{\text{move}}$  for the energy cost per bit moved, respectively for dense data movements and sparse data movements, where typically  $\tilde{E}^{\text{move}} > \bar{E}^{\text{move}}$  due to the overheads of finer-grained dynamic data handling. For weights, the energy per access ( $E^{\text{weight}}$ ) is assumed identical for SNNs and their corresponding QNNs due to matched network architecture and weight precision; the primary difference lies in the *number* of weight accesses.

The data movement energy for QNNs, considering both sparse ( $\tilde{E}_{QNN}^d$ ) and dense ( $\bar{E}_{QNN}^d$ ) activation transfers, is for-

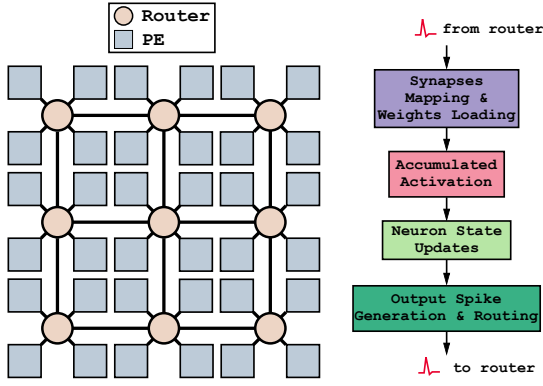


Fig. 2: A classical neuromorphic processing element (PE) array with a Network-on-Chip (NoC) for inter-core communication [21], [23], [24].

mulated as:

$$\tilde{E}_{\text{QNN}}^d = N_{\text{src}} \cdot (1 - \gamma) \cdot \underbrace{([\log_2(T + 1)] \cdot \tilde{E}^{\text{move}} + E^{\text{weight}})}_{\text{activation}} \quad (5)$$

$$\bar{E}_{\text{QNN}}^d = N_{\text{src}} \cdot ([\log_2(T + 1)] \cdot \bar{E}^{\text{move}} + E^{\text{weight}}) \quad (6)$$

Similarly, for SNNs, which transmit 1-bit spikes over  $T$  timesteps with an average spike rate  $s_r$ :

$$\tilde{E}_{\text{SNN}}^d = N_{\text{src}} \cdot T \cdot s_r \cdot (\tilde{E}^{\text{move}} + E^{\text{weight}}) \quad (7)$$

$$\bar{E}_{\text{SNN}}^d = N_{\text{src}} \cdot T \cdot (\bar{E}^{\text{move}} + E^{\text{weight}}) \quad (8)$$

We consider the actual data movement energy for each network,  $E_{\text{QNN}}^d$  and  $E_{\text{SNN}}^d$ , is the minimum of its sparse and dense options, i.e. using sparsity only if it is beneficial<sup>3</sup>.

Comparing dense transfers (Eq. (6) and Eq. (8)),  $\bar{E}_{\text{QNN}}^d$  is generally lower than  $\bar{E}_{\text{SNN}}^d$  due to the QNN processing  $[\log_2(T + 1)]$ -bit activations once, while the SNN effectively processes  $T$  individual 1-bit potential spike slots. Thus, SNN energy advantages in data movement hinge on effective sparsity utilization, as captured by  $\tilde{E}_{\text{SNN}}^d$  (Eq. (7)).

To analyze when SNNs outperform QNNs in data movement energy, we compare  $\tilde{E}_{\text{SNN}}^d$  against both  $\tilde{E}_{\text{QNN}}^d$  (sparsity-utilizing QNN) and  $\bar{E}_{\text{QNN}}^d$  (dense QNN). We define a factor  $F(\lambda)$  based on:

$$F(\lambda) = \frac{[\log_2(T + 1)] \cdot \lambda + E^{\text{weight}}}{\tilde{E}^{\text{move}} + E^{\text{weight}}} \quad (9)$$

where  $\lambda$  represents the per-bit energy cost for QNN activation movement ( $\tilde{E}^{\text{move}}$  or  $\bar{E}^{\text{move}}$ ). The conditions for SNN data movement superiority ( $\tilde{E}_{\text{SNN}}^d \leq E_{\text{QNN}}^d$ ) under three SNN spike rate ( $s_r$ ) scenarios are:

- **Best-case SNN** ( $s_r = \frac{1-\gamma}{T}$ ):  $\tilde{E}_{\text{SNN}}^d$  is always  $\leq \tilde{E}_{\text{QNN}}^d$  due to superior temporal sparsity exploitation. Compared to a dense QNN ( $\bar{E}_{\text{QNN}}^d$ ), the SNN is more efficient if:

$$\gamma \geq 1 - F(\bar{E}^{\text{move}}). \quad (10)$$

<sup>3</sup>We omit partial sum energy, as it involves local accumulator register accesses, which are negligible compared to the dominant SRAM/buffer accesses. We also ignore static (leakage) energy, assuming a platform with ultra-low-leakage cells where dynamic energy costs are dominant.

- **Average-case SNN** ( $s_r = \frac{(1-\gamma)(1/T+1)}{2}$ ): SNN surpasses sparsity-utilizing QNN ( $\tilde{E}_{\text{QNN}}^d$ ) when:

$$T \leq 2F(\tilde{E}^{\text{move}}) - 1. \quad (11)$$

Compared to a dense QNN ( $\bar{E}_{\text{QNN}}^d$ ), the condition is:

$$T \leq \frac{2F(\bar{E}^{\text{move}})}{1 - \gamma} - 1. \quad (12)$$

- **Worst-case SNN** ( $s_r = 1 - \gamma$ ): SNN outperforms sparsity-utilizing QNN ( $\tilde{E}_{\text{QNN}}^d$ ) if:

$$T \leq F(\tilde{E}^{\text{move}}). \quad (13)$$

Against a dense QNN ( $\bar{E}_{\text{QNN}}^d$ ), the requirement is:

$$T \leq \frac{F(\bar{E}^{\text{move}})}{1 - \gamma}. \quad (14)$$

## IV. RESULTS

This section presents the quantitative analyses of energy consumption based on the analytical formulas of each part from the previous section. We will use the ratio between the SNN energy and its twin QNN energy  $E_{\text{SNN}}/E_{\text{ANN}}$  as the primary factors to indicate the SNN's energy efficiency.

In section IV-A, we consider three typical software scenarios (different time steps length  $T$  and spike rate  $s_r$ ) and three hardware settings of the energy cost of the data movements, and we conduct the energy efficiency comparison under the nine combinations to evaluate the energy efficiency of SNN with respect to the twin-QNN.

Section IV-B provides a finer-grained sensitivity analysis on the effect of the SNN network parameters to its energy consumption, providing more practical design guidance for the SNN models.

The mapping of the models on the hardware system is a challenging task and might result in different distance (in terms of number of hops among cores) for data transfers across the cores, or resulting in different data reuse scenarios for both SNN and QNNs. Section IV-C further compare the QNN-SNN for different weight reuse scenario and the number of hops, providing insights into the effect of mapping on the energy trade-offs.

### A. Energy Efficiency Landscape Across Diverse Configurations

In this section, we evaluate the combinations of three typical software scenarios and three hardware settings; then compare the energy efficiency of SNNs and QNNs under these conditions.

The three SNN model configurations vary in their time window size  $T$  and spike rate  $s_r$  while the size of models are fixed to  $N_{\text{src}} = 4096$  [25]. We note that with respect to the changes in  $T$  and  $s_r$ , the bit-width of the QNN changes accordingly (Theorem 1 and Theorem 2, respectively). These cases are chosen to model scenarios ranging from highly efficient, sparse SNNs to less optimized, more active networks, with the typical case reflecting parameters common in state-of-the-art literature [7], [26]–[29]. In practice, these different

model parameters need to be chosen with respect to the deployment power constraint and the application requirement of the model performance. Concretely, the three cases are:

- 1) **Efficient SNN** ( $T = 2, s_r = 0.02$ ): Models an idealized SNN with a short time window and very low spike rate, representing a best-case scenario for SNN energy performance.
- 2) **Typical SNN** ( $T = 4, s_r = 0.1$ ): Reflects parameters common in well-known SNN architectures like DIET-SNN [26], VR-SNN [27], and Spikingformer [7], serving as a realistic baseline.
- 3) **High-Performance SNN** ( $T = 32, s_r = 0.20$ ): This configuration represents SNNs where achieving high task accuracy is prioritized, a goal that often correlates with longer integration windows and higher spike rates. For instance, state-of-the-art models like Sorbet [10] achieve high performance on GLUE benchmarks while operating with a spike rate of approximately 20% ( $s_r = 0.2$ ). This scenario allows us to analyze the energy implications of such accuracy-focused SNN designs. For thus CV tasks, TCS-SNN and RMP-SNN both adapt time window size of 32-64 to achieve a higher detecting accuracy [28], [29].

We also consider three hardware configurations: a theoretical minimum (to isolate algorithmic costs), a typical neuromorphic setting (to model a realistic implementation), and a theoretical worst sparse processing case (a condition least favorable to SNNs).

- 1) **Theoretical Minimum:** Sets all data movement and dynamic control costs to zero ( $\bar{E}^{\text{move}} = 0, \tilde{E}^{\text{move}} = 0$ ), isolating the fundamental energy of computation and static weight access.
- 2) **Typical Neuromorphic:** This setting models a realistic deployment on specialized hardware. We adopt a sparse data movement energy cost inspired by Intel’s Loihi neuromorphic chip, setting  $\tilde{E}^{\text{move}} = 3.0$  pJ/bit/hop. This number is an averaged energy cost reported for Loihi 1 [30], including the overhead for transferring metadata such as the routing information. The dense data movement cost,  $\bar{E}^{\text{move}} = 0.25$  pJ/bit/hop, is based on our own measurements for a circuit-switch NoC on a commercialized 22nm process. We assume a mapping where adjacent layers are placed on adjacent cores, resulting in a hop count of 1.
- 3) **Worst-Case for Sparse Processing:** This scenario models a hardware configuration fundamentally hostile to event-driven processing, representing the least favorable condition for SNNs. To model this high-energy context, we assume that every 1-bit spike necessitates a full 64-bit word read from off-chip DRAM, the most energy-intensive memory tier in our analysis. Based on energy values for a 64-bit DRAM access (approx. 1300 pJ [14]), the effective per-bit cost for a sparse access becomes an extreme  $\tilde{E}^{\text{move}} = 1300$  pJ/bit. The corresponding dense data movement cost is the amortized value,  $\bar{E}^{\text{move}} = 1300/64 \approx 20.3$  pJ/bit.

For efficient SNN configurations (top two rows), the energy advantage over a QNN (the “Best case” scenario) can actu-

ally increase when moving from the Theoretical Minimum to the Typical Neuromorphic setting. This occurs because the added data movement costs penalize the multi-bit QNN activations compared to the 1-bit SNN spikes. However, any potential SNN advantage is eliminated and reversed under the Worst-sparse-processing hardware scenario, where extreme overheads on sparse processing overwhelm SNN benefits. This landscape view clearly illustrates that SNN energy efficiency is not absolute but a conditional property emerging from a complex interplay of algorithmic choices and hardware realities, motivating the fine-grained parameter study in the next section.

### B. Sensitivity Analysis of Neural Network Parameters

Following the broad overview of the energy landscape, this section presents a fine-grained sensitivity analysis to quantify the impact of individual neural network parameters on energy consumption. For this study, we fix the hardware assumptions to the **Typical Neuromorphic** setting, as it represents a realistic deployment scenario for specialized accelerators. This allows us to isolate the effects of intrinsic model characteristics.

Against a fixed, optimized QANN baseline with 80% activation sparsity [31], we systematically vary key SNN parameters—time window ( $T$ ), spike rate ( $s$ ), weight precision (4-bit and 8-bit), and network size ( $N_{\text{src}}$ )—to quantify their influence on the energy ratio  $E_{\text{SNN}}/E_{\text{QANN}}$ . Figure 5 presents the results of this parametric sweep.

**Impact of Time Window ( $T$ ) and SNN Spike Rate ( $s_r$ ):** A primary observation is that as  $T$  increases, the SNN must operate at an increasingly lower spike rate ( $s_r$ ) to remain energy-competitive with the QNN. For instance, with 8-bit weights and  $N_{\text{src}} = 4096$ , the breakeven point where  $E_{\text{SNN}} = E_{\text{QNN}}$  occurs at  $s_r \approx 0.3$  for  $T = 1$ , but this threshold tightens significantly to  $s_r \approx 0.046$  for  $T = 7$ . This trend is expected, as the SNN’s dominant energy costs scale with the  $T \cdot s_r$  product, while the QNN’s energy cost increases more slowly with the QNN precision of  $\lceil \log_2(T + 1) \rceil$ .

However, our analysis reveals a nuanced exception when transitioning from  $T = 7$  to  $T = 8$ . The breakeven spike rate for  $T = 7$  ( $s_r \approx 0.046$ ) is slightly lower (i.e., more stringent) than for  $T = 8$  ( $s_r \approx 0.0049$ ). This counter-intuitive result occurs because the QNN’s precision requirement jumps from 3 bits ( $\lceil \log_2(7 + 1) \rceil$ ) to 4 bits ( $\lceil \log_2(8 + 1) \rceil$ ), causing a step increase in its  $E_{\text{MAC}}$ . The SNN’s energy increase from one additional timestep is less pronounced, making it comparatively more efficient at  $T = 8$  than at  $T = 7$ . Despite this local anomaly, the overarching conclusion remains that larger  $T$  values impose severe constraints on the operational spike rate for SNNs to maintain an energy advantage.

Furthermore, Figure 5 highlights a critical threshold for the SNN’s internal data transmission strategy. For the Typical Neuromorphic setting, this threshold occurs at  $s_r \approx 0.12 - 0.17$ , depending on weight bit-width. When the SNN spike rate  $s_r$  exceeds this value, the energy cost of handling sparse events ( $N_{\text{src}} T s_r (\tilde{E}^{\text{move}} + E_{\text{weight}})$ ) surpasses that of broadcasting data densely ( $N_{\text{src}} T (\bar{E}^{\text{move}} + E_{\text{weight}})$ ). This indicates that for

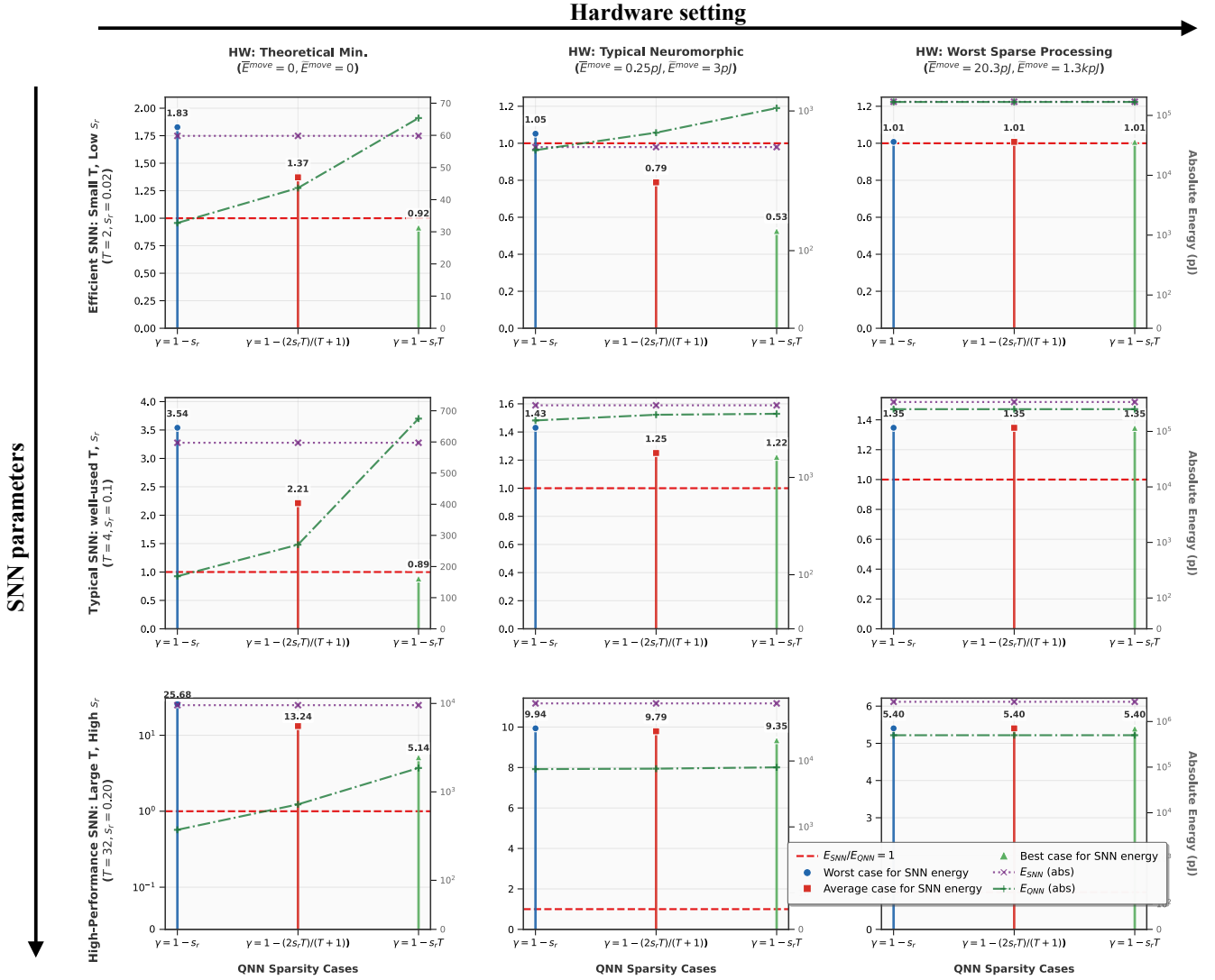


Fig. 3: Energy ratio  $E_{SNN}/E_{ANN}$  across SNN Model Configurations (rows, defined by  $T, s_r$ ) and Hardware Settings (columns). Within each cell, three bars correspond to comparing the SNN against QNNs with three activation densities. All calculations assume  $N_{src} = 4096$  and 8-bit weights. Fundamental operational costs are:  $E_{ACC} = 0.05448$  pJ,  $E_{CMP} = 0.05448$  pJ,  $E_{SUB} = 0.05448$  pJ. The QNN  $E_{MAC}$  cost varies with  $T$  as detailed in Figure 4. These energy values are based on a 22nm technology process.

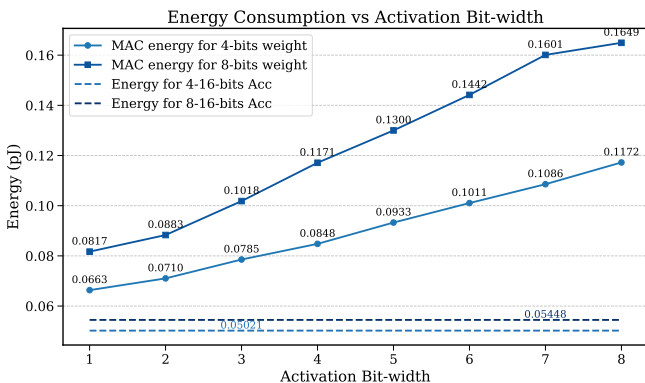


Fig. 4: Mac vs Acc

higher-activity SNNs, a dense dataflow can be more energy-efficient than a sparse, event-driven one within the same architecture.

**Impact of Network Size ( $N_{src}$ ):** To evaluate scalability, we compare SNN/QNN efficiency for a small network ( $N_{src} = 64$ ) versus a larger network ( $N_{src} = 4096$ ), using both 4-bit and 8-bit weights and varying  $T$  and  $s_r$  (Figure 5). While absolute energy values scale significantly with  $N_{src}$  (as most dominant energy terms are proportional to  $N_{src}$ ), the relative efficiency trends and the  $s_r$  break-even points do not drastically change. For example, for  $T = 5$  and 4-bit weights, the SNN-QNN breakeven  $s_r$  is 0.058 for  $N_{src} = 4096$  and remains similar at 0.057 for  $N_{src} = 64$ . This suggests that while  $N_{src}$  dictates the magnitude of energy consumption, its impact on the *relative* SNN vs. QNN efficiency ranking (for a given  $T, s_r$ ) is much

Hyperparameters setting

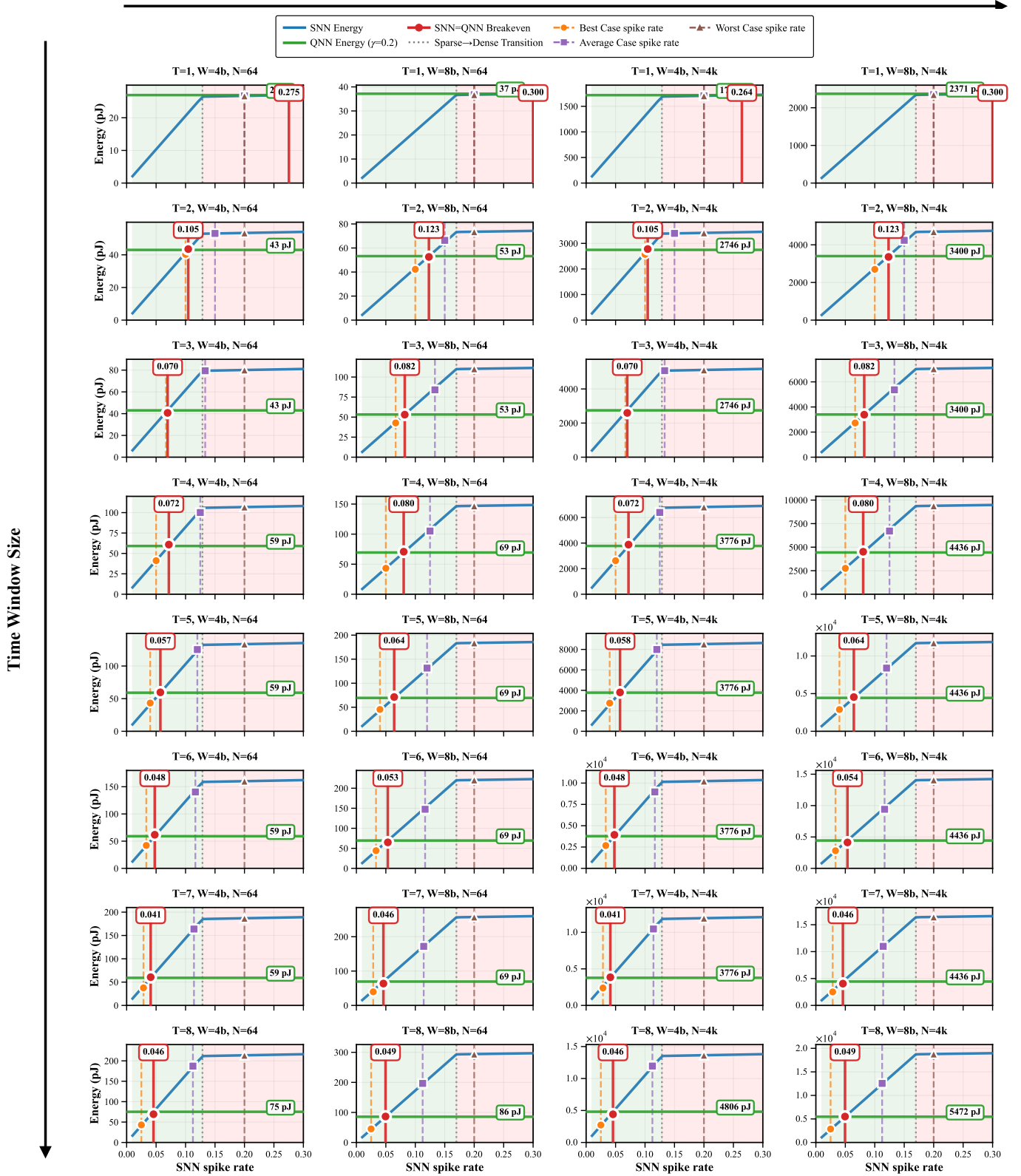


Fig. 5: Sensitivity analysis of SNN and QNN energy consumption (pJ) versus SNN spike rate ( $s_r$ ) under the Typical Neuromorphic hardware setting ( $\bar{E}^{move} = 0.25$  pJ/bit/hop,  $\bar{E}^{move} = 3$  pJ/bit/hop, number of hop equal to 1). Each subplot corresponds to a specific SNN time window  $T$  (rows,  $T \in [1, 8]$ ) and a configuration of weight precision (4-bit or 8-bit) and network size ( $N_{src} \in \{64, 4096\}$ ) (columns). QNN energy (horizontal line) is calculated for a fixed activation sparsity of  $\gamma = 0.8$ .

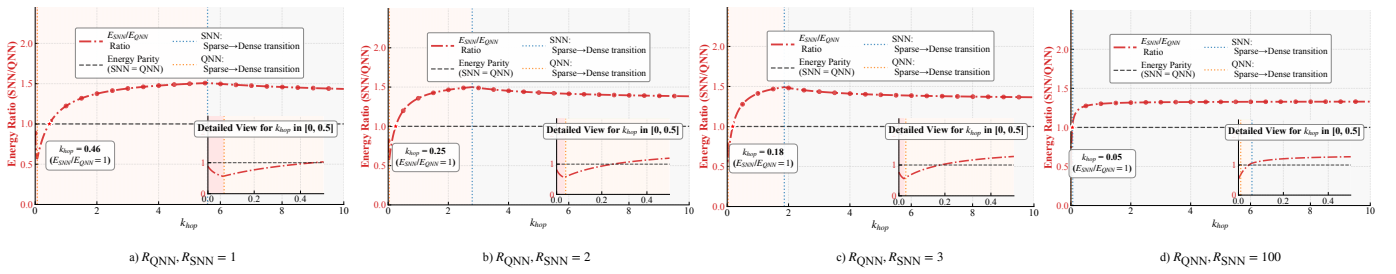


Fig. 6: Ablation studies for number of hops

less pronounced than that of  $T$  or  $s_r$  itself.

**Impact of Weight Precision:** Increasing weight precision relaxes the sparsity requirement for an SNN to achieve energy parity with a QNN, allowing the SNN to remain competitive at higher spike rates ( $s_r$ ). For instance, in our evaluation with  $T = 2$  and  $N_{\text{src}} = 4096$ , the breakeven spike rate  $s_r$  increases from 0.105 for 4-bit weights to 0.123 for 8-bit weights. This trend is because higher precision disproportionately increases the energy of a QNN’s MAC operations relative to an SNN’s ACCs, amplifying the SNN’s efficiency. While both architectures consume more power at higher precision, the QNN’s baseline energy rises more sharply than the SNN’s energy. This dominant effect shifts the energy crossover point, making the SNN advantageous over a wider operational range.

**Overall Insights:** Our sensitivity analysis identifies the SNN time window size and spike rate as the most critical algorithmic parameters governing relative energy efficiency. Our results quantify a clear trade-off: as  $T$  increases, the permissible spike rate for an SNN to remain energy-competitive shrinks dramatically. Under typical neuromorphic settings, our analysis shows that for SNNs to be more efficient than a comparable QNN, **the spike rate ( $s_r$ ) must be kept below 5.4% once the time window ( $T$ ) exceeds five timesteps**. This highlights the paramount importance of co-designing SNN models to operate with both short time windows and extreme sparsity.

### C. Analyses on the effect of mapping

1) *Modeling routing distance of data movements:* In previous setting, we assumed adjacent layers are placed on adjacent cores, implying a hop count of 1. However, to provide a more comprehensive and realistic analysis, we relax the fixed hop count assumption by introducing  $k_{\text{hop}}$ , a scaling factor representing the average number of inter-core hops per transfer. This allows us to model a range of scenarios: from a best-case intra-core mapping ( $k_{\text{hop}} = 0$ ), to our baseline assumption ( $k_{\text{hop}} = 1$ ), to a worst-case routing across the chip (e.g.,  $k_{\text{hop}}$  being a large number). We incorporated this  $k_{\text{hop}}$  factor by scaling the base data movement costs,  $\tilde{E}^{\text{move}}$  and  $\bar{E}^{\text{move}}$ , showing in Equation 17-20.

2) *Modeling weight reuse :* The degree of weight reuse is highly dependent on many factors, including the dataflow mapping, the system configuration, and model parameters (e.g., hidden dimension, batch size, sequence length). This complexity makes it intractable to model a precise reuse value, as it is highly compiler and hardware specific. Therefore, to

provide a more robust and sound energy analysis without attempting to model exact, mapping-specific reuse schemes, we introduce two weight reuse factors,  $R_{\text{QNN}}$  and  $R_{\text{SNN}}$ , which scale the weight-reading energy ( $E^{\text{weight}}$ ), as shown in Equation 17-20. For both SNN and QNN, the worst-case scenario (no reuse) corresponds to  $R = 1$ . Conversely, an optimal buffering strategy (e.g., reusing weights across a large batch and sequence length) would yield a large  $R$ , driving this component of the energy cost toward zero. For SNNs, although they suffer from sparse and irregular memory access patterns [32], they still have opportunities for weight reuse. For example, previous SNN designs [33]–[35] employ temporal-parallel execution, allowing weights to be reused across the time window.

Considering these two factors—routing complexity and weight reuse—we now rewrite the data movement equations as follows:

$$\tilde{E}_{\text{QNN}}^d = N_{\text{src}} \cdot (1 - \gamma) \cdot \underbrace{([\log_2(T + 1)] \cdot (k_{\text{hop}}) \cdot \tilde{E}^{\text{move}})}_{\text{activation}} + \frac{E^{\text{weight}}}{R_{\text{QNN}}} \quad (15)$$

$$\bar{E}_{\text{QNN}}^d = N_{\text{src}} \cdot ([\log_2(T + 1)] \cdot (k_{\text{hop}}) \cdot \bar{E}^{\text{move}} + \frac{E^{\text{weight}}}{R_{\text{QNN}}}) \quad (16)$$

$$\tilde{E}_{\text{SNN}}^d = N_{\text{src}} \cdot T \cdot s_r \cdot ((k_{\text{hop}}) \cdot \tilde{E}^{\text{move}} + \frac{E^{\text{weight}}}{R_{\text{SNN}}}) \quad (17)$$

$$\bar{E}_{\text{SNN}}^d = N_{\text{src}} \cdot T \cdot ((k_{\text{hop}}) \cdot \bar{E}^{\text{move}} + \frac{E^{\text{weight}}}{R_{\text{SNN}}}) \quad (18)$$

We further perform a sensitivity analysis on  $k_{\text{hop}}$  and the reuse factor, assuming a typical SNN, neuromorphic setting and a QNN density of  $\gamma = 1 - s_r T$  (Section III.A, best-case SNN).

3) *Analysis results on the number of hops  $k_{\text{hop}}$ :* We first analyze the  $E_{\text{SNN}}/E_{\text{QNN}}$  energy ratio as a function of  $k_{\text{hop}}$ , setting various values of  $R_{\text{QNN}} = R_{\text{SNN}} = R$  from 1 to 100. Figure 6 plots the energy ratio as a function of  $k_{\text{hop}}$ . SNNs are more beneficial to sparse activations due to its capability of leveraging bit-level sparsity while QNNs are relatively more suitable to dense data movements. As our energy model uses the best energy consumption between sparse and dense data movements of activations, the SNN/QNN energy ratio is dictated by the transition from sparse to dense transfers of the activations of both SNN and QNN. For example, at  $R = 1$

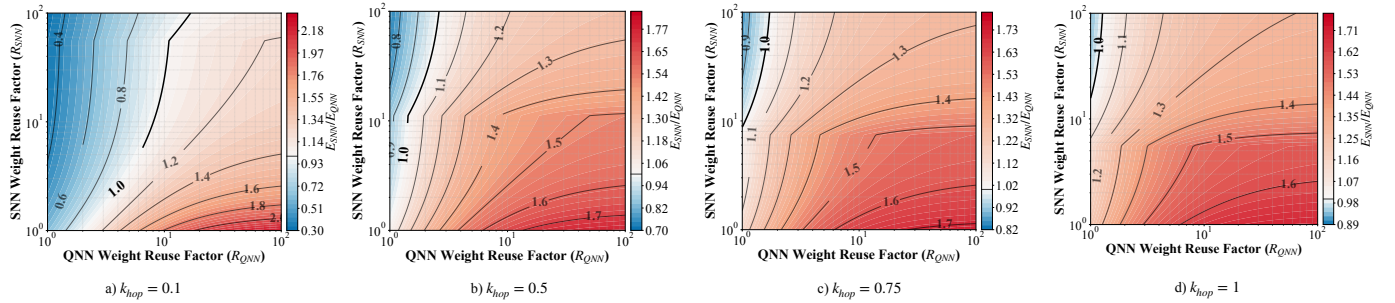


Fig. 7: Weight reuse factors 2D heatmap. Each subplot (a-d) corresponds to a fixed routing cost,  $k_{hop}$ , ranging from 0.1 to 1. A ratio below 1.0 (blue) indicates the SNN is more energy-efficient, while a ratio above 1.0 (red) favors the QNN.

(no reuse), the ratio first decreases to  $\approx 0.5$  (favoring SNN) while the QNN uses sparse movement. As  $k_{hop}$  increases, the data movements cost increases, the QNN’s cost model would prefer dense data movements, causing the  $E_{SNN}/E_{QNN}$  ratio to increase.

However, with the increase of the reuse factor  $R$ , the energy of moving weight are less important in the overall energy and hence the dense data transfers become preferable at lower value of number of hops  $k_{hop}$ . Quantitatively, as  $R$  increases from 1 to 100, the breakeven  $k_{hop}$  value drops from 0.44 to just 0.04. Thus, high weight reuse (a large  $R$ ) makes it significantly harder for SNNs to achieve energy efficiency relative to QNNs. To outperform a QNN with  $R = 100$ , the SNN with same reuse factor must be mapped with an average hop count of  $k_{hop} < 0.04$ , which is extremely hard to meet; especially considering that meeting such low number of hops usually require the mapping to group a considerable amount of neurons into the same core which reduces the parallelism and hence detracts the performance.

4) *Analysis results on the reuse factor:* Figure 7 plots the SNN/QNN energy ratio for different weight reuse factor of SNN and QNN. The color indicates this ratio, where SNN wins in the blue zone and QNN in the red zone and the darkness of the colors indicates the quantitative ratio. Figure 7.a) to c) vary in  $k_{hop}$ . The high-level trends are intuitive: increasing  $R_{QNN}$  (moving right in each figure) degrades the SNN’s relative energy efficiency, while increasing  $R_{SNN}$  (moving up) improves it. However, the trends from (a) to (d) reveal a critical interaction with the hop count,  $k_{hop}$ . At low  $k_{hop}$  values (e.g., 0.1), SNNs have more chances to be more energy efficient than QNNs. The core reason is at low  $k_{hop}$ , the cost of moving activation becomes negligible compared to the cost of loading weights (see Equation 15-18), and hence leveraging sparsity proportionally reduces the total energy of loading weights for both SNN and QNN, so both SNN and QNN prefer to operate in sparse mode, but SNN better benefits sparsity due to its capability of leveraging bit-level sparsity. Conversely, as  $k_{hop}$  increases, the energy of reading weights becomes a negligible part of the total cost and hence both SNN and QNN would prefer to operate in the dense mode where SNN does not benefit from its sparsity and becomes harder to beat its twin-QNN.

D. Ablation study over VGG16

To empirically prove this theoretical equivalence on real-world data, we evaluate QNN-to-SNN conversion using VGG16<sup>4</sup>. We first train the networks with quantization function derived from Lemma 2 for 100 epochs with a learning rate of 1e-3 on a single NVIDIA A100 GPU (PyTorch 1.12.1+cu116). Then, we transfer the weight of QNN to SNN and let SNN do the inference. Table I reports accuracy and sparsity for both QNN and SNN across time steps ( $T$ ) 3 to 8. The results show the SNN achieves near-identical accuracy to its QNN counterpart. The accuracy difference on CIFAR-100 is consistently below 0.2% in all configurations, and in several cases (e.g., CIFAR-10 at  $T = 7$ ), the SNN slightly outperforms the QNN. This empirically confirms the conversion is effectively lossless.

TABLE I: QNN vs. SNN accuracy and sparsity for VGG16 on CIFAR10 and CIFAR100 across time steps  $T$ .

Metric	Time Steps ( $T$ )					
	3	4	5	6	7	8
<b>CIFAR100 / VGG16</b>						
QNN accuracy(%)	63.31	69.91	71.52	72.16	72.26	72.80
SNN accuracy(%)	63.24	69.72	71.43	72.08	72.45	72.97
QNN avg. density rate (%)	15.39	21.52	26.34	29.45	32.30	34.30
SNN avg. spike rate (%)	7.09	8.39	9.50	10.04	10.69	10.94
<b>CIFAR10 / VGG16</b>						
QNN accuracy (%)	81.73	90.86	92.16	93.01	93.09	92.93
SNN accuracy (%)	82.09	90.71	91.82	92.93	93.11	92.94
QNN avg. density rate (%)	12.20	16.52	19.89	22.98	25.45	27.39
SNN avg. spike rate(%)	5.49	6.43	7.10	7.73	8.19	8.52

Lastly, we evaluate the total energy for the trained VGG16 model on CIFAR-10. For this analysis, we set the average hop count  $k_{hop} = 1$ . We define  $N_{src}$  as the layer fan-in (input channels  $\times$  kernel size<sup>2</sup>) and set the reuse factors as follows:  $R_{QNN} = H_{out} \times W_{out}$ , modeling full spatial reuse of each kernel, while  $R_{SNN} = T \times H_{out} \times W_{out}$  to account for the SNN’s ability to additionally exploit temporal reuse across the  $T$  time steps. Table II compares the final activation density and energy for both QNN and SNN. The results show that the SNN only achieves a slight energy advantage (Ratio=0.9823) at a low time step ( $T = 3$ ), where its spike rate is minimal

<sup>4</sup>VGG16 structure: [64\*2, A, 128\*2, A, 256\*3, A, 512\*3, A, 512\*3, A], where A denotes an average pooling layer and 64, 128, etc., are the channel counts.

TABLE II: Energy and activation density comparison between SNN and QNN models on CIFAR-10, measured across varying simulation timesteps ( $T$ ).

Timesteps ( $T$ )	Activation Density (%)		Energy (pJ)		Energy Ratio (SNN/QNN)
	QNN	SNN	SNN	QNN	
3	12.22	5.49	1204.72	1226.38	0.9823
4	16.52	6.43	1881.21	1839.32	1.0228
5	19.89	7.10	2596.45	1847.54	1.4054
6	22.98	7.73	3392.12	1855.07	1.8286
7	25.45	8.19	4192.91	1861.09	2.2529
8	27.39	8.52	4880.81	2474.34	1.9726

(5.49%). As  $T$  and the spike rate increase, the QNN quickly becomes more efficient. This finding is consistent with our previous analysis.

## V. DISCUSSION

### A. Future of SNN

From our perspective, the future trajectory of spiking neural networks diverges into two primary directions. The first centers around purely brain-inspired methodologies—algorithmic innovations and neuromorphic hardware—to emulate the functionalities of the human brain [36]. Despite significant exploration, brain-inspired algorithms consistently fall short compared to conventional neural networks enhanced by GPU acceleration, especially in terms of performance, speed, and scalability. Indeed, the closer an algorithm or hardware implementation approximates biological realism, the narrower its practical applicability typically becomes. For example, while contemporary AI research pushes boundaries with large language models containing hundreds of billions of parameters, SNN research frequently remains restricted to simplistic benchmarks such as CIFAR10. This disparity underscores a critical question regarding the genuine necessity of SNNs. A key factor limiting their broader adoption is the absence of training algorithms tailored specifically for spiking neuron dynamics; current methods predominantly borrow from ANN paradigms, such as rate-coded surrogate-gradient backpropagation. Therefore, fundamentally novel learning frameworks that align naturally with the discrete, temporal behavior inherent in spiking neurons are essential to fully realize SNNs’ potential. Furthermore, to validate SNNs’ practicality relative to ANNs, careful selection of application domains is crucial, particularly focusing on inherently asynchronous, event-driven data streams like neuromorphic sensor inputs, real-time robotics, and signals from hardware components such as memristors [37]. Recent research also shows that SNNs have chance to perform better in terms of energy on temporal tasks instead of static tasks by comparing state-of-the-art hardware accelerators [38].

The second promising direction involves cross-fertilizing traditional neural network methodologies, GPU-based acceleration techniques, and brain-inspired computing paradigms to achieve superior energy efficiency without sacrificing performance [39]. Viewed from this angle, SNNs share conceptual similarities with bit-level quantized ANNs. Our analyses highlight scenarios, particularly ultra-low-power (ULP) applications supported by specialized hardware, where SNNs exhibit

notable energy efficiency benefits over quantized ANNs [40]. Furthermore, hybrid architectures combining optimized ANN and SNN layers tailored to their respective computational strengths represent an exciting avenue for innovation. These hybrid models offer significant architectural flexibility, effectively harnessing each paradigm’s unique capabilities to optimize computational efficiency and overall model performance.

### B. SNN aggregated transmission

As discussed in Section III-B, the timestep-level transmission strategy (SNN) exploits fine-grained temporal sparsity by transmitting spike events individually at each timestep. However, this approach incurs the cost of sending the full spike train of length  $T$  without compression. In contrast, aggregated transmission strategies (SNN’) have recently gained popularity [27], [41]. For instance, in rate encoding, a spike train of length  $T$  can encode spike counts from 0 to  $T$  using only  $\log_2(T + 1)$  bits; specifically, a spike train with  $T = 7$  timesteps can represent spike counts (0–7) with just 3 bits, greatly reducing transmission overhead. Although this aggregated approach significantly reduces data volume, it sacrifices the opportunity to exploit sparsity at the individual timestep level. The only case in which timestep-level sparsity is effectively leveraged is when the spike train contains no spikes at all, allowing the entire transmission to be skipped. Consequently, the effective sparsity for such aggregated methods is determined not by the spike rate, but rather by the activation-level sparsity  $\gamma$ , analogous to QNNs. The corresponding data movement energy equations for aggregated transmission are:

$$\tilde{E}_{\text{SNN}'}^d = \underbrace{N_{\text{src}} \cdot (1 - \gamma)}_{\text{spike rate matches ANN density}} \cdot (\log_2 T \cdot \tilde{E}^{\text{move}} + E^{\text{weight}}) \quad (19)$$

$$\bar{E}_{\text{SNN}'}^d = N_{\text{src}} \cdot (\log_2 T \cdot \bar{E}^{\text{move}} + E^{\text{weight}}) \quad (20)$$

Since these aggregated encoding schemes share identical data movement costs with QNNs, they underscore the structural similarity between SNNs and QNNs. Moreover, given comparable per-bit movement energies, the choice between uncompressed (timestep-level) and compressed (aggregated) spike train transmission ultimately reduces to a critical trade-off: whether the spike-level sparsity in the SNN is sufficiently high to achieve greater energy efficiency than the aggregated approach, characterized by its compressed  $\log_2 T$ -bit representation.

### C. SNN potential on existing low power devices

To contextualize our analytical findings, we translate the per-inference energy costs into a tangible metric: the operational lifetime of a wearable device. We consider a typical smartwatch with a 4000-Joule (1.1 Wh) battery [42], executing one network layer inference per cycle at a frequency of 100 MHz [40], [43], [44]. The device lifetime is calculated as:

$$\text{Lifetime} = \frac{\text{Battery Capacity}}{E_{\text{inference}} \times \text{Frequency}}$$

In an optimized scenario, using our “Efficient SNN” configuration ( $T = 2, s = 0.02$ ) under a “typical neuromorphic hardware”, the energy per inference is 551.35 pJ. This translates to a device lifetime of approximately 20.2 hours. In contrast, its twin QNN, consuming 1048.41 pJ per inference, would yield a lifetime of only 10.6 hours, demonstrating a potential  $1.9\times$  improvement with the SNN.

However, this advantage is not guaranteed and is critically dependent on the network’s operational parameters. If we consider the “High-Performance SNN” configuration ( $T = 32, s = 0.20$ ), its high operational cost results in a device lifetime of merely 0.15 hours—less than 10% of the runtime achievable by its corresponding twin QNN. This example starkly illustrates our central finding: while SNNs offer a pathway to substantial energy savings, these benefits are only realized through careful co-design of the algorithm and hardware to ensure operation within an efficient, low-activity regime.

## VI. CONCLUSION

This paper addresses the conditions under which spiking neural networks achieve better energy efficiency compared to equivalent quantized ANNs. Through an analysis grounded in a fair comparison between models with equivalent information representation, we find that SNN energy efficiency is not a given, but requires a confluence of favorable algorithmic and hardware properties. At a high level, the design space for energy-efficient SNNs depends on achieving a low total number of spike events (a low  $T \cdot s$  product), hardware optimized for low-cost sparse event processing (minimal  $\tilde{E}^{\text{move}}$ ), and a substantial MAC-to-ACC energy ratio ( $E_{\text{MAC}} \gg T \cdot E_{\text{ACC}}$ ). Our analysis provides specific design guidance based on these factors. For instance, under typical neuromorphic hardware settings, we recommend that for an SNN to be selected, its time window should be kept below four timesteps ( $T < 4$ ) with a spike rate below approximately 7%. Beyond these operational points, a well-optimized QNN is often the more energy-efficient choice. In summary, this work provides a quantitative framework to guide model selection and emphasizes the necessity of algorithm-hardware co-design for realizing the energy-saving potential of SNNs.

## REFERENCES

- [1] J. K. Eshraghian, M. Ward, E. O. Neftci, X. Wang, G. Lenz, G. Dwivedi, M. Bennamoun, D. S. Jeong, and W. D. Lu, “Training spiking neural networks using lessons from deep learning,” *Proceedings of the IEEE*, 2023.
- [2] C. Ganguly and S. Chakrabarti, “A discrete time framework for spike transfer process in a cortical neuron with asynchronous epsp, ipsp, and variable threshold,” *IEEE Transactions on Neural Systems and Rehabilitation Engineering*, vol. 28, no. 4, pp. 772–781, 2020.
- [3] B. Rueckauer, I.-A. Lungu, Y. Hu, M. Pfeiffer, and S.-C. Liu, “Conversion of continuous-valued deep networks to efficient event-driven networks for image classification,” *Frontiers in Neuroscience*, vol. 11, p. 682, 2017.
- [4] X. Wu, Y. Zhao, Y. Song, Y. Jiang, Y. Bai, X. Li, Y. Zhou, X. Yang, and Q. Hao, “Dynamic threshold integrate and fire neuron model for low latency spiking neural networks,” *Neurocomputing*, vol. 544, p. 126247, 2023.
- [5] R. B. Stein, E. R. Gossen, and K. E. Jones, “Neuronal variability: noise or part of the signal?” *Nature Reviews Neuroscience*, vol. 6, no. 5, pp. 389–397, 2005.
- [6] R. Brette, “Philosophy of the spike: rate-based vs. spike-based theories of the brain,” *Frontiers in systems neuroscience*, vol. 9, p. 151, 2015.
- [7] C. Zhou, L. Yu, Z. Zhou, Z. Ma, H. Zhang, H. Zhou, and Y. Tian, “Spikingformer: Spike-driven residual learning for transformer-based spiking neural network,” *arXiv preprint arXiv:2304.11954*, 2023.
- [8] M. Bal and A. Sengupta, “Spikingbert: Distilling bert to train spiking language models using implicit differentiation,” in *Proceedings of the AAAI conference on artificial intelligence*, vol. 38, no. 10, 2024, pp. 10 998–11 006.
- [9] X. Xing, Z. Zhang, Z. Ni, S. Xiao, Y. Ju, S. Fan, Y. Wang, J. Zhang, and G. Li, “Spikelm: Towards general spike-driven language modeling via elastic bi-spiking mechanisms,” *arXiv preprint arXiv:2406.03287*, 2024.
- [10] K. Tang, Z. Yan, and W.-F. Wong, “Sorbet: A neuromorphic hardware-compatible transformer-based spiking language model,” *arXiv preprint arXiv:2409.15298*, 2024.
- [11] M. Dampfhofer, T. Mesquida, A. Valentian, and L. Anghel, “Are snns really more energy-efficient than anns? an in-depth hardware-aware study,” *IEEE Transactions on Emerging Topics in Computational Intelligence*, vol. 7, no. 3, pp. 731–741, 2022.
- [12] Z. Yan, J. Zhou, and W.-F. Wong, “Cq++ training: Minimizing accuracy loss in conversion from convolutional neural networks to spiking neural networks,” *IEEE Transactions on Pattern Analysis and Machine Intelligence*, vol. 45, no. 10, pp. 11 600–11 611, 2023.
- [13] W. A. Wulf and S. A. McKee, “Hitting the memory wall: Implications of the obvious,” *ACM SIGARCH computer architecture news*, vol. 23, no. 1, pp. 20–24, 1995.
- [14] M. Horowitz, “1.1 computing’s energy problem (and what we can do about it),” in *2014 IEEE international solid-state circuits conference digest of technical papers (ISSCC)*. IEEE, 2014, pp. 10–14.
- [15] Y.-H. Chen, T.-J. Yang, J. Emer, and V. Sze, “Eyeriss v2: A flexible accelerator for emerging deep neural networks on mobile devices,” *IEEE Journal on Emerging and Selected Topics in Circuits and Systems*, vol. 9, no. 2, pp. 292–308, 2019.
- [16] W. Wei, M. Zhang, J. Zhang, A. Belatreche, J. Wu, Z. Xu, X. Qiu, H. Chen, Y. Yang, and H. Li, “Event-driven learning for spiking neural networks,” *arXiv preprint arXiv:2403.00270*, 2024.
- [17] J. Vasiljevic, L. Bajic, D. Capalija, S. Sokorac, D. Ignjatovic, L. Bajic, M. Trajkovic, I. Hamer, I. Matosevic, A. Cejkov *et al.*, “Compute substrate for software 2.0,” *IEEE micro*, vol. 41, no. 2, pp. 50–55, 2021.
- [18] S. Lie, “Cerebras architecture deep dive: First look inside the hw/sw co-design for deep learning: Cerebras systems,” in *2022 IEEE Hot Chips 34 Symposium (HCS)*. IEEE Computer Society, 2022, pp. 1–34.
- [19] R. Prabhakar, S. Jairath, and J. L. Shin, “Sambanova sn10 rdu: A 7nm dataflow architecture to accelerate software 2.0,” in *2022 IEEE International Solid-State Circuits Conference (ISSCC)*, vol. 65. IEEE, 2022, pp. 350–352.
- [20] Z. Yan, J. Zhou, and W.-F. Wong, “Near lossless transfer learning for spiking neural networks,” in *Proceedings of the AAAI conference on artificial intelligence*, vol. 35, no. 12, 2021, pp. 10 577–10 584.
- [21] A. Lines, P. Joshi, R. Liu, S. McCoy, J. Tse, Y.-H. Weng, and M. Davies, “Loihi asynchronous neuromorphic research chip,” *Energy*, vol. 10, no. 15, pp. 10–1109, 2018.
- [22] F. Akopyan, J. Sawada, A. Cassidy, R. Alvarez-Icaza, J. Arthur, P. Merolla, N. Imam, Y. Nakamura, P. Datta, G.-J. Nam *et al.*, “Truenorth: Design and tool flow of a 65 mw 1 million neuron

- programmable neurosynaptic chip,” *IEEE transactions on computer-aided design of integrated circuits and systems*, vol. 34, no. 10, pp. 1537–1557, 2015.
- [23] D. S. Modha, F. Akopyan, A. Andreopoulos, R. Appuswamy, J. V. Arthur, A. S. Cassidy, P. Datta, M. V. DeBole, S. K. Esser, C. O. Otero *et al.*, “Neural inference at the frontier of energy, space, and time,” *Science*, vol. 382, no. 6668, pp. 329–335, 2023.
- [24] C. Pehle, S. Billaudelle, B. Cramer, J. Kaiser, K. Schreiber, Y. Stradmann, J. Weis, A. Leibfried, E. Müller, and J. Schemmel, “The brainscales-2 accelerated neuromorphic system with hybrid plasticity front,” 2022.
- [25] H. Touvron, T. Lavril, G. Izacard, X. Martinet, M.-A. Lachaux, T. Lacroix, B. Rozière, N. Goyal, E. Hambro, F. Azhar *et al.*, “Llama: Open and efficient foundation language models,” *arXiv preprint arXiv:2302.13971*, 2023.
- [26] N. Rathi and K. Roy, “Diet-snn: A low-latency spiking neural network with direct input encoding and leakage and threshold optimization,” *IEEE Transactions on Neural Networks and Learning Systems*, vol. 34, no. 6, pp. 3174–3182, 2023.
- [27] Z. Yan, K. Tang, J. Zhou, and W.-F. Wong, “Low latency conversion of artificial neural network models to rate-encoded spiking neural networks,” *IEEE Transactions on Neural Networks and Learning Systems*, pp. 1–12, 2025.
- [28] B. Han and K. Roy, “Deep spiking neural network: Energy efficiency through time based coding,” in *European conference on computer vision*. Springer, 2020, pp. 388–404.
- [29] B. Han, G. Srin, and K. Roy, “Rmp-snn: Residual membrane potential neuron for enabling deeper high-accuracy and low-latency spiking neural network,” in *Proceedings of the IEEE/CVF conference on computer vision and pattern recognition*, 2020, pp. 13 558–13 567.
- [30] M. Davies, N. Srinivasa, T.-H. Lin, G. Chinya, Y. Cao, S. H. Choday, G. Dimou, P. Joshi, N. Imam, S. Jain *et al.*, “Loihi: A neuromorphic manycore processor with on-chip learning,” *Ieee Micro*, vol. 38, no. 1, pp. 82–99, 2018.
- [31] R. Gong, Y. Yong, Z. Wang, J. Guo, X. Wei, Y. Ma, and X. Liu, “Fast and controllable post-training sparsity: Learning optimal sparsity allocation with global constraint in minutes,” in *Proceedings of the AAAI Conference on Artificial Intelligence*, vol. 38, no. 11, 2024, pp. 12 190–12 198.
- [32] H. Lee, C. Kim, S. Lee, E. Baek, and J. Kim, “An accurate and fair evaluation methodology for snn-based inferencing with full-stack hardware design space explorations,” *Neurocomputing*, vol. 455, pp. 125–138, 2021.
- [33] J.-J. Lee, W. Zhang, and P. Li, “Parallel time batching: Systolic-array acceleration of sparse spiking neural computation,” in *2022 IEEE International Symposium on High-Performance Computer Architecture (HPCA)*. IEEE, 2022, pp. 317–330.
- [34] R. Yin, Y. Kim, D. Wu, and P. Panda, “Loas: Fully temporal-parallel dataflow for dual-sparse spiking neural networks,” in *2024 57th IEEE/ACM International Symposium on Microarchitecture (MICRO)*. IEEE, 2024, pp. 1107–1121.
- [35] R. Mao, L. Tang, X. Yuan, Y. Liu, and J. Zhou, “Stellar: Energy-efficient and low-latency snn algorithm and hardware co-design with spatiotemporal computation,” in *2024 IEEE International Symposium on High-Performance Computer Architecture (HPCA)*. IEEE, 2024, pp. 172–185.
- [36] G. Li, L. Deng, H. Tang, G. Pan, Y. Tian, K. Roy, and W. Maass, “Brain-inspired computing: A systematic survey and future trends,” *Proceedings of the IEEE*, 2024.
- [37] N. Ghoshal and B. Tripathy, “Real-time visual data processing using neuromorphic systems,” in *Primer to Neuromorphic Computing*. Elsevier, 2025, pp. 161–183.
- [38] F. Ottati, C. Gao, Q. Chen, G. Brignone, M. R. Casu, J. K. Eshraghian, and L. Lavagno, “To spike or not to spike: A digital hardware perspective on deep learning acceleration,” *IEEE Journal on Emerging and Selected Topics in Circuits and Systems*, vol. 13, no. 4, pp. 1015–1025, 2023.
- [39] J.-H. Lee, S.-H. Hwang, W. Jo, K.-U. Byeon, and J.-K. Han, “Time-to-first-spike coding in sensory neuron for energy-efficient spiking neural networks,” *IEEE Electron Device Letters*, 2025.
- [40] Z. Yan, Z. Bai, T. Mitra, and W.-F. Wong, “Sparrowsnn: A hardware/software co-design for energy efficient eeg classification,” *arXiv preprint arXiv:2406.06543*, 2024.
- [41] X. Xing, B. Gao, Z. Zhang, D. A. Clifton, S. Xiao, L. Du, G. Li, and J. Zhang, “Spikellm: Scaling up spiking neural network to large language models via saliency-based spiking,” *arXiv preprint arXiv:2407.04752*, 2024.
- [42] J. Huang, A. Badam, R. Chandra, and E. B. Nightingale, “{WearDrive}: Fast and {Energy-Efficient} storage for wearables,” in *2015 USENIX Annual Technical Conference (USENIX ATC 15)*, 2015, pp. 613–625.
- [43] H. Chu, Y. Yan, L. Gan, H. Jia, L. Qian, Y. Huan, L. Zheng, and Z. Zou, “A neuromorphic processing system with spike-driven snn processor for wearable eeg classification,” *IEEE Transactions on Biomedical Circuits and Systems*, vol. 16, no. 4, pp. 511–523, 2022.
- [44] H. A. Gonzalez, S. Muzaffar, J. Yoo, and I. M. Elfadel, “Biocnn: A hardware inference engine for eeg-based emotion detection,” *IEEE Access*, vol. 8, pp. 140 896–140 914, 2020.



**Zhanglu Yan** received the BSc degree in Computer Science from Xi’an Jiaotong University in 2019, the MSc degree in Artificial Intelligence from the National University of Singapore (NUS) in 2020, and the PhD degree in Computer Science from NUS in 2024. He is currently a research fellow at NUS. His research focuses on neuromorphic computing and spiking neural networks.



**Zhenyu Bai** is a Research Fellow in the Department of Computer Science, National University of Singapore. His research interests include spatial dataflow architectures design and compilation techniques.



**Kaiwen Tang** Kaiwen Tang received the BSc degree in computer science from Xi’an Jiaotong University in 2022. She is working toward the PhD degree in the School of Computing, National University of Singapore. Her research focuses on spiking neural networks and efficient language models.



**Wong Weng-Fai** received the BSc degree from the National University of Singapore, in 1988, and the DrEngSc degree from the University of Tsukuba, Japan, in 1993. He is currently an associate professor with the Department of Computer Science, National University of Singapore. His research interests include computer architecture, compilers, and high-performance computing. He is a senior member of the IEEE.